ACS APPLIED MATERIALS & INTERFACES

RESEARCH ARTICLE

www.acsami.org

Multi-Layered Plasma-Polymerized Chips for SPR-Based Detection

Ram P. Gandhiraman,[*,†] Nam Cao Hoai Le,[†,▽] Chandra K. Dixit,[‡] Cedric Volcke,[§] Colin Doyle,[⊥] Vladimir Gubala,[†] Suresh Uppal,[#] Ruairi Monaghan,[†] Bryony James,[§] Richard O'Kennedy,[†,‡] Stephen Daniels,[†,#] and David E. Williams[||]

[†]Biomedical Diagnostics Institute (BDI), [‡]School of Biotechnology, and [#]School of Electronic Engineering, Dublin City University, Glasnevin, Dublin-9, Ireland

[§]Research Centre in Physics of Matter and Radiation (PMR), University of Namur (FUNDP), 61, rue de Bruxelles, B-5000 Namur, Belgium

[⊥]Research Centre for Surface and Materials Science, Department of Chemical and Materials Engineering, [||]MacDiarmid Institute for Advanced Materials and Nanotechnology, Department of Chemistry, University of Auckland, Private Bag 92019, Auckland 1142, New Zealand

Supporting Information

ABSTRACT:

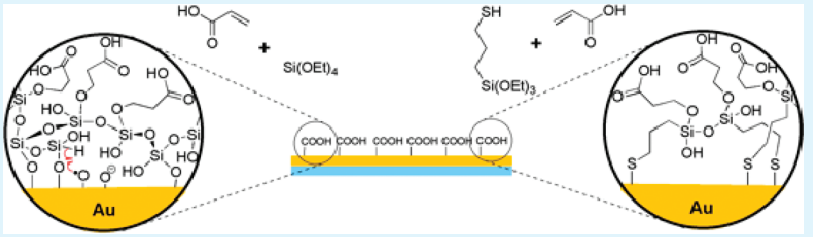

The surface functionalization of a noble metal is crucial in a surface plasmon resonance-based biomolecular detection system because the interfacial coating must retain the activity of immobilized biomolecules while enhancing the optimal loading. We present here a one-step, room-temperature, high-speed, gas-phase plasma polymerization process for functionalizing gold substrates using siloxane as an adhesion layer and acrylic acid as a functional layer. Siloxane- and thiol-based coatings were compared for their performance as adhesion and the interfacial layer for subsequent functionalization. An in situ sequential deposition of siloxane and acrylic acid resulted in a 7-fold increase in carboxylic functionality surfacial content compared to films deposited with thiol-containing precursors. Grading of the layer composition achieved as a consequence of ion-induced mixing on the surface coating under the application of the plasma is confirmed through secondary ion mass spectroscopic studies. DNA hybridization assays were demonstrated on gold/glass substrates using surface plasmon enhanced ellipsometry and the applicability of this coating for protein immunoassays were demonstrated with plasma functionalized gold/plastic substrates in Biacore 3000 SPR instrument.

KEYWORDS: PECVD, surface functionalization, SPR, biomolecule immobilization, ellipsometry

INTRODUCTION

The use of surface-based immunoassays for biomolecular detection rapidly increased in the recent past by employing techniques enabling high-sensitivity detection transducers. Much research has been focused on improving both the detection surfaces and techniques. Particularly, surface plasmon resonance (SPR) and related techniques represent a unique category of real-time and label-free analytical tools that allow the users to study specific biological and chemical interactions between receptors and analytes in solution, and to perform sensitive and specific assays.[1−3] High-sensitivity detection by SPR is carried out by exciting plasmon surface polaritons at the interface between a metal film and a dielectric medium. An evanescent field propagates along the metal/dielectric interface and the optical reflectivity is sensitively controlled by changes in the refractive index of the medium within the penetration depth of the evanescent field. By using the resultant evanescent waves that propagate along the metal/dielectric interface, the optical properties of the ultrathin films deposited at the metal surface can be studied. By knowing the sequential change in optical properties upon introduction of chemical or biological samples, specific chemical or biomolecular species present in the sample can be qualitatively but also quantitatively detected. A critical step in any SPR-based assay is to immobilize a biomolecule onto a noble metal surface while retaining its biological activity and an accessibility of active sites toward analytes to be detected.[4] In this context, chemisorption is the most commonly used strategy for biomolecules immobilization.[5,6] Covalent binding, which makes use of interfacial layers, is

Received: August 8, 2011
Accepted: October 26, 2011
Published: October 26, 2011

preferable in order to gain optimum protein loading along with maximum biological activity.[5] For example, covalent immobilization of biomolecules onto gold substrates is routinely performed through wet chemical methods including thiol-coupling chemistry, functionalized dextran or the use of gamma-aminopropylethoxysilane, as reported by several research groups.[7−9] To achieve good batch-to-batch reproducibility, factors such as reaction temperature, concentration of the reagents, stirring rate, and humidity must be precisely controlled. Moreover, the formation of alkanethiol self-assembled monolayers, for example, onto gold substrate is a time-consuming process that requires immersion of the substrate in thiol solutions for longer duration ranging from 18 to 48 h.[10,11] The large amount of solvents, with a resulting increase in solvent wastes, makes the wet chemistry techniques less attractive if bulk quantities of coated substrates with high quality are required. Alternatively, the use of gas-phase processes such as plasma-enhanced chemical vapor deposition (PECVD) could overcome such drawbacks and represent a class of relatively straightforward, quick method capable to functionalize different substrates with a large range of surface chemistries presenting tailored surface characteristics.[12−14] Particularly, plasma-enhanced chemical vapor deposition (PECVD), a high-speed, dry, highly controllable, routine industrial manufacturing process, would evidently be preferable if the correct chemistry is available.

In this context, Szunerits et al., reported room-temperature deposition of organosilicon film on gold at room temperature by PECVD of tetramethyldisiloxane[15] and deposition of silicon oxide on gold by PECVD at an elevated temperature of 300 °C.[16] They also reported on the sputter deposited ITO protective layer on gold for SPR measurements.[17] More recently, Touahir et al. reported PECVD deposition of amorphous silicon−carbon alloys at 250 °C.[18] However, further functionalization to facilitate biomolecule immobilization was carried out by liquid-phase deposition. A recent review on surface functionalization strategies of SPR chips has been presented by Wijaya et al.[19] Point-of-care diagnostics using microfluidics for sample handling and SPR-based detection are mainly made of gold coated plastics,[20−22] that normally have low glass transition temperature, especially polycarbonates and cyclo olefin copolymers and hence low temperature deposition is critical. To the best of our knowledge, plasma polymerization of reactive functionalities onto gold surfaces has not been reported either at high- or low-temperature. Particularly, in this paper, deposition of mercaptopropyltrimethoxysilane (MPTMS) by plasma polymerization was explored. Indeed, the mercapto functionality can serve as an adhesion layer while the siloxane network can be used as a building layer for further modification. Sequential deposition of MPTMS and acrylic acid (AA) is proposed to create carboxyl functionalization of gold. Another alternate and inexpensive functionalization process was also explored using another siloxane layer (based on tetraethylorthosilicate, TEOS) and acrylic acid. The effect of siloxane intermediate layer on the plasma polymerization and in reducing the nonspecific binding of biomolecules through formation of silanols is discussed elsewhere.[23] Surface characteristics of acrylic acid coatings deposited on cyclo olefin polymers, with and without underlying siloxane intermediate layer showed that the amount of carboxy functionalities is 2.5 times higher when an intermediate layer is present. Moreover, the nonspecific binding is lower with the presence of an intermediate layer. Indeed, plasma polymerization of TEOS is a well-established process in semiconductor industry. Moreover, it is easy to handle compared to mercaptosilane and film characteristics are more easily tailored through precise control of plasma process parameters.

In this work, a low-temperature deposition of carboxylic functionalities on gold by PECVD using sequential deposition of a suitable adhesion layer and acrylic acid is reported. The use of both thiol-based and non thiol-based coatings is explored and their surface characterization is carried out using both qualitative and quantitative analysis. The plasma polymerization was carried out on both gold on glass and gold on plastic substrates and their performance in SPR based bioassays has been demonstrated using surface plasmon enhanced ellipsometry for DNA hybridization and Biacore 3000 for IgG-based bioassays.

EXPERIMENTAL SECTION

Materials and Reagents. Gold-coated standard glass slides (Ti/Au = 2 nm/48 nm, 26 mm × 76 mm, 1 mm thick) were purchased from Phasis Sarl (Geneva, Switzerland). Tetraethylorthosilicate (TEOS) $Si(OC_2H_5)_4$, acrylic acid (AA) CH_2═CHCOOH, 3-mercaptopropyltrimethoxysilane (MPTMS) $HS(CH_2)_3Si(OCH_3)_3$, N-(3-dimethylaminopropyl)-N′-ethylcarbondiimide hydrochloride (EDC), and N-hydroxysuccinimide (NHS) were purchased from Sigma-Aldrich (Dublin, Ireland). All chemicals were used as received without further purification. Amino-modified single-stranded DNAs (5′-CGC-CAA-TAT-TTA-CGT-GCT-GCT-A −3′) (miR-16 probe, 22-mer), complementary single-stranded DNAs or microRNA (5′-U-AGC-AGC-ACG-UAA-AUA-UUG-GCG-3′) (miR-16 target, 22-mer) and noncomplementary single-strand DNAs or microRNA (5′-UAG-CAG-CAC-AGA-AAU-AUU-GGC-3′) (miR-195 target, 21-mer) were purchased from Eurofins MWG Operon (Ebersberg, Germany). Goat antimouse IgG and mouse IgG were purchased from Sigma Aldrich (Dublin, Ireland). CM5 Biacore chips were purchased from GE Lifesciences, UK.

PECVD System. The deposition of multilayered carboxy functional coatings was carried out in a computer controlled PECVD reactor Europlasma, model CD300 (Oudenaarde, Ghent, Belgium). An aluminum vacuum chamber, connected to a Dressler CESAR 136 RF power source (Munsterau, Stolberg, Germany) with an operating frequency of 13.56 MHz, with an automated impedance-matching box, was used. The details of the deposition system are provided elsewhere.[24] The bare gold slides were cleaned with dry air and then loaded in the chamber. The chamber was pumped to a base pressure of 20 mTorr. The liquid precursors (TEOS, MPTMS, Acrylic acid) were stored in stainless steel containers connected to the chamber through quarter-inch steel tubes and needle valve. The liquids were stored in three individual containers and each controlled separately through needle valve.

Magnetron Sputtering of Gold on Polycarbonate. The gold deposition was carried out in a homemade magnetron sputtering system. A 2 in.-diameter gold target from Kurt J Lesker was used as a target. The polycarbonate substrates were loaded in the chamber and the system was pumped down to 1×10^{-6} mbar. A 5 sccm argon flow was then introduced and the plasma was ignited using a pulsed DC power supply source at 75 W. The operating pressure was 2×10^{-3} mbar and the deposition time was 5 min. The resultant gold thickness was about 40 nm.

Deposition. The samples were loaded in the plasma chamber and pumped down to a base pressure of 20 mTorr. For nonthiol based, TEOS + acrylic acid (so-called TA coating) film deposition, 50 sccm of argon and 50 sccm of oxygen were introduced. The plasma was then ignited with an RF power of 30 W. The plasma pretreatment was carried out for 40 s. It is a known phenomenon that the plasma pretreatment at low pressure removes the contaminants and also improves adhesion of the coating. The oxygen flow was stopped and the RF power was reduced to 14 W. TEOS was then introduced and siloxane deposition

was carried out for 3 min in argon and TEOS plasma. TEOS flow was then stopped and acrylic acid was introduced in the chamber. The carboxylic deposition was carried out in argon and acrylic acid plasma for 30 s at 14 W. In the case of MPTMS+Acrylic acid (so-called MA coating) deposition, a plain argon plasma pretreatment was carried out at 30 W for 40 s. Oxygen flow was avoided during pretreatment in order to favor thiol-gold interaction. The RF power was then reduced to 14 W. MPTMS was introduced and mercapto silane deposition was carried out for 30 s in argon and MPTMS plasma. MPTMS flow was then stopped and acrylic acid was introduced in the chamber. The carboxylic deposition was carried out in argon and acrylic acid plasma for 30 s at 14 W. The need for plasma process control to retain the functionality has been reported elsewhere.[25] The plasma power is kept to a minimum in order to retain the monomer functionality.

X-ray Photoelectron Spectroscopy (XPS). The XPS data were collected on a Kratos Axis UltraDLD equipped with a hemispherical electron energy analyzer. Spectra were excited using monochromatic Al Kα X-rays (1486.69 eV) with the X-ray source operating at 100 W. This instrument illuminates a large area on the surface and then using hybrid magnetic and electrostatic lenses collects photoelectrons from a desired location on the surface. In this case the analysis area was a 220 × 220 μm spot. The measurements were carried out in a normal emission geometry. A charge neutralization system was used to alleviate sample charge buildup, resulting in a shift of approximately 3 eV to lower binding energy. Survey scans were collected with a 160 eV pass energy, while core level scans were collected with a pass energy of 20 eV. The analysis chamber was at pressures in the 1×10^{-9} Torr range throughout the data collection. Data analysis was performed using CasaXPS version 2.3.15 (www.casaXPS.com). Shirley backgrounds were used in the peak fitting. Quantification of survey scans utilized relative sensitivity factors supplied with the instrument. Core level data were fitted using Gaussian−Lorentzian peaks (30% Lorentzian). The binding energy scale was corrected for the neutralizer shift by using the C 1s signal from saturated hydrocarbon at 285.0 eV as an internal standard. The elements present in the coating C, N, O, Si, S were detected using the XPS survey scan (see the Supporting Information, Figure S1). High-resolution scans of individual core levels show the various bonding states of each elements.

Polarization-Modulation Infrared Reflection Absorption Spectroscopy (PMIRRAS). PMIRRAS spectra were recorded on a Bruker Equinox 55-PMA37 spectra equipped with liquid nitrogen cooled mercury cadmium-telluride (MCT) detector and a zinc-selenide photoelastic modulator. The infrared light was modulated between s- and p-polarization at a frequency of 50 kHz. The incident angle upon the sample surface was around 85°. Signals generated from each polarization (Rs and Rp) were detected simultaneously by a lock-in amplifier and used to calculate the differential surface reflectivity $(\Delta R/R) = (R_p - R_s)/(R_p + R_s)$. The spectra were an average of 640 scans and were taken at a spectral resolution of 2 cm^{-1}.

Contact Angle. The film wettability was analyzed by measuring the water contact angle of the film surface (First Ten Angstroms FTA200 contact angle analyzer). High-purity HPLC grade water (Sigma Aldrich) was used for the measurement.

Atomic Force Microscopy (AFM). Atomic force microscopy (AFM) was used to compare the topographical surface of TA and MA with bare Au-coated glass substrates. A Digital Instruments (DI) BioScopeTM II (Veeco Instruments Inc., Plainview, NY, USA) operating in tapping mode under ambient conditions was used. Images were acquired with silicon cantilevers with integrated tips (TESP, Veeco Probes, Camarillo, CA, USA) and with resonant frequencies between 327 and 349 kHz, and with ~30 N/m spring constant. Samples were analyzed over a 1 μm × 1 μm sample area at a resolution of 512 × 512 pixels and at a scan rate of 0.5 Hz. Images were produced from raw data using Research NanoScope 7.30 software (Veeco Instruments Inc., Plainview, NY, USA). Zero-order plane fitting was used to remove the image bow that can result from the scanner moving out-of-plane with the sample. The root-mean-square roughness (R_{rms}) was defined as the average of height deviations taken from the mean plane.[26]

Spectroscopic Ellipsometry. The thickness of the films deposited on the sensing substrate was measured by a spectroscopic ellipsometer (UVISEL, Jobin Yvon Horiba, France) in external mode. PsiDelta 2 software was used for fitting the data from the measured Ψ and Δ spectra.

Surface Plasmon Enhanced Ellipsometry. Total internal reflection ellipsometry (TIRE) or surface plasmon enhanced ellipsometry (SPEE) is a spectroscopic ellipsometry measurement method operated under total internal reflection (TIR) condition.[27] Similar to conventional spectroscopic method, SPEE also measure two ellipsometric angles Ψ and Δ versus wavelengths. These Ψ and Δ values are defined by the ratio ρ of the reflection coefficients R_p and R_s for components of light polarized parallel (p) and perpendicular (s) to the plane of incidence following the ellipsometry equation

$$\rho = \frac{R_p}{R_S} = \tan \Psi \exp(i\Delta)$$

where Rp and Rs are the electric field reflection coefficients for *p* and *s* polarized lights. It is obvious that Ψ and Δ also depend on angle of incidence Φ and wavelengths λ. The refractive indices and thicknesses of each layer of the reflecting surfaces can be found by fitting the measured Ψ and Δ data to a defined model. The SPEE measurements were conducted at an angle of incidence of approximately 68.3° with wavelengths ranging from 350 to 1000 nm. The integration time was 200 ms and the spectral resolution was 3 nm. PsiDelta 2 software (Jobin Yvon Horiba, France) was used for fitting the data from the measured Ψ and Δ spectra from SPEE. First, we tested the stability of the TA or MA films on the Au-coated glass substrate inside one of the microwells by replacing new PBS buffer every 60 min in a 360 min period during which four sets of Ψ and Δ were recorded separated by 60 min. These sets of Ψ and Δ spectra were used in the ellipsometric fitting with 4-layer model to obtain the film thicknesses.

For the purpose of estimating the thickness changes of the TA or MA film upon contact with buffer solution and upon binding with DNA, a four-layer model similar to the model used in[28] was used in the fitting of measured TIRE spectra. In this model, the refractive indices of the TA, MA films and the DNA film are assumed to follow the same Cauchy dispersion formula ($A + B/\lambda^2 + C/\lambda^4$, $A = 1.415$, $B = 0.01$ nm^2, $C = 0$) obtained from ref 29, because the refractive indices of tetraethyl orthosilicate, mercaptosilane, acrylic acid, and DNA are relatively close. This assumption inevitably compromised the determination of the exact refractive index of each film but it helped to uncouple the refractive indices and film thicknesses in ellipsometric fitting. Furthermore, it also helps to minimize the difficulty in fitting for the thicknesses of several of films of very close refractive indices.[30−32]

The DNA hybridization assay was conducted in a fresh microwell after the baseline Ψ and Δ spectra of the TA or MA surface in PBS buffer were recorded. Eighty microliters of aminated miR-16 probe at a concentration of 1 μM in 100 mM EDC in 2-(N-morpholino)-ethanesulfonic acid (MES, pH 8.0) buffer was pumped into the microwell and allowed to react for 60 min with continuous pumping at a flow-rate of approximately 1.3 μL/min. A second set of Ψ and Δ spectra, which correspond to the registration of the binding of the capture miR-16 probe, were measured after the microwell was rinsed with 50 μL of PBS buffer. Next, 80 μL of complementary miR-16 target at concentration of 1 μM in hybridization buffer (2 × concentrate buffer with SSC, Sigma H7140) was pumped into the microwell at the same flow-rate and also allowed to react for 60 min before rinsing with 50 μL PBS. A third set of Ψ and Δ spectra were then recorded corresponding to the hybridization of the complementary miR-16 target to the capture

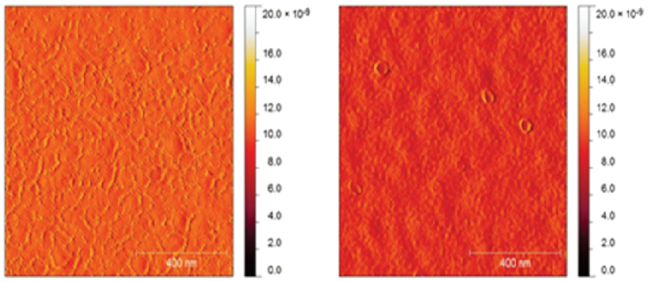

Figure 1. Atomic force microscopic image of TA (left) and MA (right) on gold.

miR-16 probe. We also conducted two negative control experiments in two different microwells. The negative control experiment was conducted with mismatched miR-195 target at concentration of 1 μM to confirm the specificity of the captured miR-16 probes. The film thickness changes after binding of the miR-16 probes and then the hybridization with the complementary miR-16 target or noncomplementary miR-195 target was measured by using the SPEE.

Surface Plasmon Resonance (SPR). The chip functionality was demonstrated with Biacore 3000 (GE Healthcare) using mouse IgG. The developed chip was docked and primed on the Biacore 3000 instrument. EDC (20 μL of 4 mg/mL) and NHS (20 μL of 8 mg/mL) were mixed in the mentioned volumes and 20 μL of the mixture was injected over the chip surface. Sixty microliter of goat antimouse IgG at a concentration of 20 μg/mL was injected in the designated flow-cell. A 3% (w/v) solution of bovine serum albumin (BSA) in 0.1 M PBS, pH 7.2 was injected to block the surface in order to minimize nonspecific interaction of analytes with the EDC-activated surface. IgG was injected at three different dilutions, i.e., 15, 35, and 70 ng/mL. The baseline was allowed to settle prior and after each sample injection. The blank control, which was performed by injecting goat IgG over the antimouse IgG-immobilized surface, was deducted from the response units (RU) obtained for captured mouse IgG. The plasma-deposited samples for both SPEE and SPR measurements were stored at room temperature in ambient atmosphere and no further treatments were carried out prior to measurements.

RESULTS AND DISCUSSION

Carboxylic acid functionalities are plasma deposited through two different interfacial layers based on TEOS or MPTMS precursors, each one followed by a subsequent deposition of acrylic acid. The sequentially deposited TEOS + acrylic acid coatings and MPTMS + acrylic acid coatings are hereafter called as TA and MA coatings, respectively. The film thickness of TA is 8 nm and that of MA is 16 nm, as measured using ellipsometry.

1. Surface and Bulk Composition. Film topography, measured using atomic force microscopy (AFM), reveals that the surface roughness of TA and MA films are 0.7 and 0.5 nm, respectively (Figure 1). Also, as the contact angle of TA is less than 10°, the surface is extremely hydrophilic. Oppositely, water contact angle of MA being 45°, the surface is less hyrophilic. Even though the film wettability ranges from extremely hydrophilic to less hydrophilic, the surface reactivity of the carboxylic functionality is retained in both the cases as shown below. The surface roughness and water contact angle of plain gold is 0.4 nm and 83°, respectively.

PM-IRRAS spectra of both TA and MA coatings contain several vibrational features that can be assigned to the deposited siloxane (1300−1000 cm^{-1} region), silanol (900−970 cm^{-1} region)

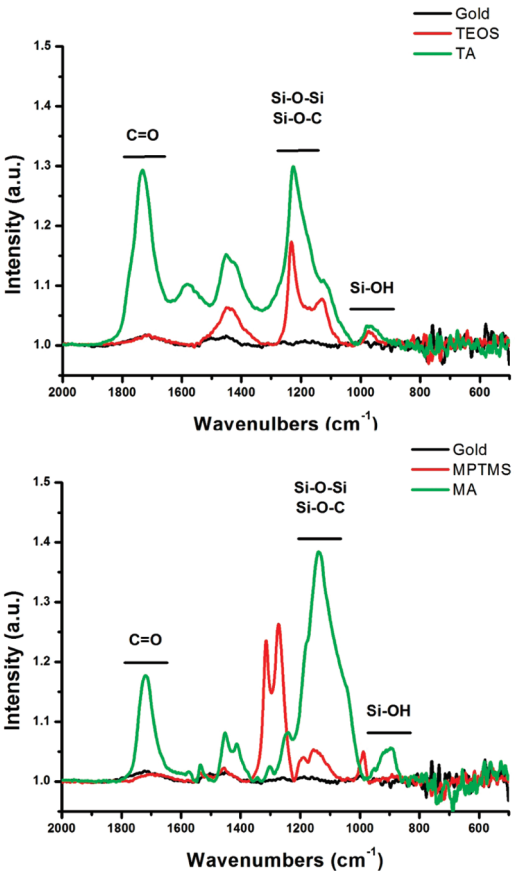

Figure 2. (Top) PMIRRAS spectra of bare gold-coated substrate (black), TEOS-coated (red), and TA-coated (green) gold surfaces. (Bottom) PMIRRAS spectra of bare gold-coated substrate (black), MPTMS-coated (red),and MA-coated (green) gold surfaces. The presence of carboxyl group is highlighted in TA and MA coatings.

Table 1. Surface Elemental Composition of TA and MA Coatings Calculated from XPS Survey Spectra (in at %)

element	TA coating %	MA coating %
Cls	35.7	48.3
Ols	40.9	27.1
S2p		7.9
Si2p	7.7	11.5
Ag3d	1.5	1.2
Au4f	14.2	4.0

and carboxyl/carbonyl (1720−1730 cm^{-1} region) species (Figure 2).[13,33,34] These infrared features are missing on the gold substrate spectrum.

The bands in the 1300−1000 cm^{-1} siloxane region can be decomposed into several peaks associated to the $\delta_s(Si\text{-}CH_3)$ deformation, $Si\text{-}CH_2\text{-}R$ deformation and Si−O−C, Si−O−Si vibrations.[35,36] It also appears as evident from Figure 2 that the presence of carboxyl/carbonyl functionality (at 1720 cm^{-1}) is due to the acrylic acid deposition as the corresponding peak intensity is insignificant on the underlying TEOS and MPTMS coatings spectra on its own. The peak at 1447 cm^{-1} corresponds to CH_3 deformation mode and the 1313 cm^{-1} in MPTMS is due to deformation modes of the CH_2 of the propylic chain.[37−39]

Table 2. Various Bonding Environment of Carbon in High-Resolution C 1s XPS Spectrum

bonds		TA coating	MA coating
C−C	%	60.8	6.8
	BE(eV)	285.0	285.0
C−S	%		50.4
	BE(eV)		285.6
C−O	%	20.2	40.1
	BE(eV)	286.5	286.5
O−C═O	%	19.0	2.7
	BE(eV)	289.1	289.0

XPS was carried out for a quantitative elemental analysis of the plasma deposited coatings. The relative elemental composition of both films is identified and quantified (Table 1) from XPS survey spectra (see the Supporting Information). Further, to study the various bonding environments, high-resolution scans of the core level photoemission spectra of C 1s, Si 2p, and S 2p were carried out. Si 2p doublet in both films corresponds to SiO_2 and Si−OH (see the Supporting Information, Figure S2).[40] As the atomic percentage of Si in MA and TA coatings are, respectively, 11.5 and 7.7%, the coating growth rate appears higher for MPTMS coatings than for TEOS at the same deposition time (Table 1). It is also observed that the atomic percentage of oxygen in TA is 40.9% and that in MA is 27.1% (Table 1).

The relative composition of carbon peak after deconvolution is detailed in Table 2. The Polymer database[41] gives the C 1s for C−S bonding in poly(hexamethylene Sulphone) at 285.64 eV, and lower for S adjacent to aromatic groups.The presence of carboxyl related peak at 289.1 eV (+ 4.1 eV) in Figure 3 (Top and Middle)[41,42] confirms previous water contact angle and PMIRRAS data. However, the carboxy content (COO/C) in TA coating (19%) is three times higher compared to the carboxy content of plain acrylic acid films reported in the literature (Table 2).[34] Moreover, a drastic reduction in carboxy content is observed in MA coating (2.7%).

Although the exact origin of this observation is not demonstrated, some hypothesis can be postulated while comparing results obtained using TEOS and MPTMS precursors. We assume it is due to a combination of two factors: the chemical composition of the precursor and the surface pretreatment applied before precursor deposition. Indeed, we can assume the difference in O−C═O content in the layer is partly due to difference in the chemical composition of the precursor. The pretraetment applied to gold surface before deposition also certainly influence results. Precisely, MPTMS contains a sulfur atom (which is not present in TEOS), as well as three oxygen atoms (compared to TEOS molecules which contains 4 oxygen atoms). Moreover, an argon+oxygen plasma pretreatment is applied before TEOS deposition, whereas it is composed only of an argon plasma before MPTMS deposition.

The postulated deposition mechanism is the following: the deposition of TEOS and AA being sequential, the oxidation and deposition of TEOS is carried out before the deposition of carboxylic functionalities from AA molecules. As an argon+oxygen plasma pretreatment was carried out, some residual oxygen would also be involved in the oxidation of TEOS molecules. Oppositely, in the MA coating, two factors are assumed to induce a depletion in oxygen content of the MPTMS coating: (1) in the case of MPTMS and MA coatings, only an argon plasma pretreatment was used (since gold−sulfur affinity is stronger than oxidized gold−siloxane affinity) and therefore no residual oxygen is available in the chamber for further precursor oxidation process; (2) MPTMS has only 3 oxygen atoms in the MPTMS precursor (4 for TEOS precursor). As there is an oxygen deficit at film MPTMS surface before performing the AA plasma (compared to TEOS film surface), it is speculated that some oxygen atoms from the AA plasma is involved in the oxidation of the interfacial components. The mass spectroscopy analysis of the AA plasma (Unpublished data) show the break up of acrylic acid molecules into highly reactive oxygen, CO and OH species. Hence the quantity of carboxy content in the resultant film is significantly lower for MA compared to that of TA.

Si 2p doublet in both TA and MA corresponds to SiO_2 and SiOH (see the Supporting Information). The growth rate being higher for Mercapto silane as compared to that of TEOS for the same deposition time, the atomic percentage of Si in MA is 11.5%

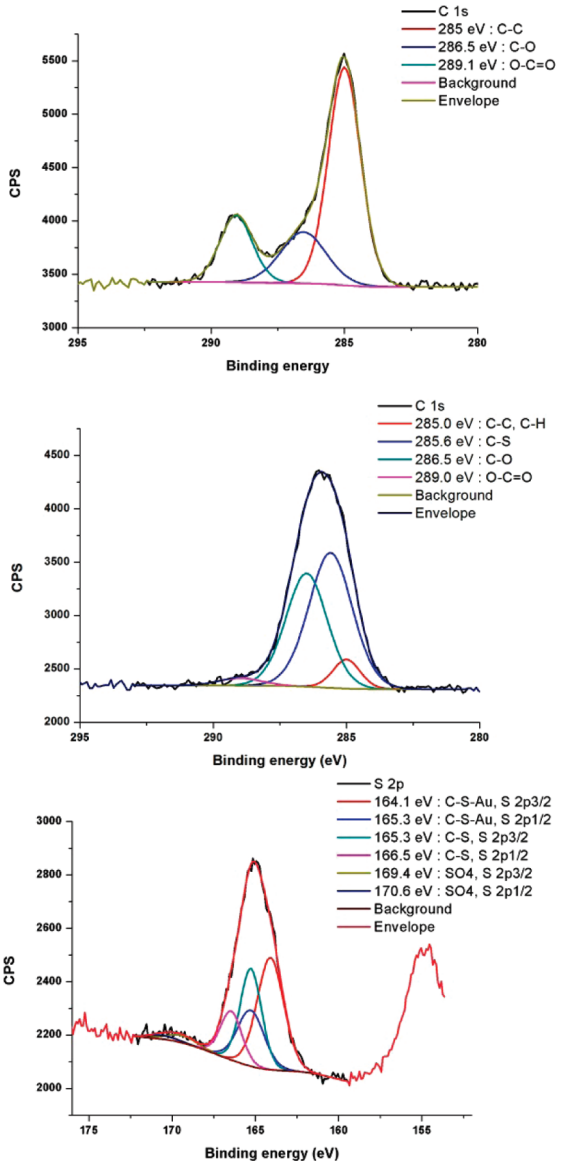

Figure 3. High-resolution core level photo electron spectroscopy of (top) C 1s of TA coating, (middle) C 1s of MA coating, (bottom) high-resolution core level photo electron spectroscopy of S 2p of MA coating.

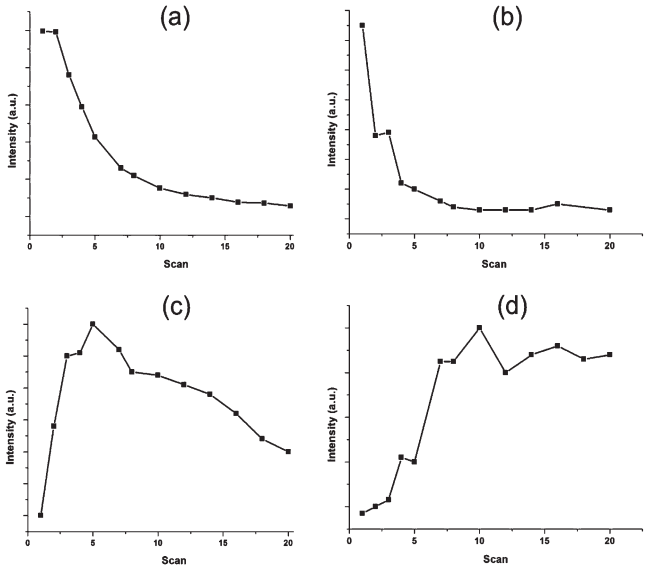

Figure 4. SIMS spectra of TA and MA coating showing the depth profile measurement. (a, b) Carbon (m/z = 12) of TA and MA coatings, respectively. (c, d) Silicon (m/z = 27.97) of TA and MA coatings, respectively.

and that of Si in TA 7.7% (Table 1). The core level S 2p spectra (Figure 3, bottom) exhibits three doublet components. The S 2p doublet at 164.1 eV can be attributed to sulfur bound to gold (Au−S) at the coating surface. The doublet at 165.3 and 166.5 eV can be attributed to S−H or S−C bonds.[43] The final doublet at 169.4 and 170.6 eV can be attributed to sulfonate ($-SO_4$) bonds.[44] It can therefore be deduced that part of the sulfur is involved in bonding with gold substrate, part of the sulfur exists as free thiol (SH, S−C) and the remaining sulfur is in its sulfonate state (bonded to four oxygen atoms).[45,46] It is reported that sulfonate bonds are not observed in freshly prepared self-assembled monolayers of MPTMS but, for old samples, oxidized sulfur species emerge.[47] This can be explained as follows: the plasma process results in the formation of highly reactive species, including atomic oxygen as observed through optical emission spectroscopy (Unpublished data). This led to the formation of sulfonate bonds between sulfur atoms from MPTMS precursors and oxygen from the plasma. Once the plasma is ignited, the precursor molecules decompose into reactive species which react together and deposit on the surface. Knowing the chemistry of introduced precursors (MPTMS and AA), we can assume the plasma to be composed at least of O−, Si−O−, $-CH_2$, −SH... So, even though no oxygen plasma pretreatment was done, the oxygen in MPTMS could have contributed for sulfonate formation in the bulk. Moreover, oxygen in carboxylic acid could also have contributed for the oxidation of the top layer of the mercapto coating, as confirmed by XPS data. Indeed, XPS studies of mercaptosilane coating on its own (without acrylic acid) confirms the presence of sulfonate bonds (see the Supporting Information, Figure S3).

The hydrocarbon chains present in both precursors (TEOS, MPTMS) are also oxidized by oxygen atoms present in the precursor and acrylic acid, creating H_2O, and/or CO_2 gaseous byproducts, which are removed by the pumping system. It is also observed that the atomic percentage of oxygen in TA is 40.9% and that in MA is 27.1% (Table 1). The plasma deposition of MPTMS however results in a sulfur mixed atmospheric environment and the gaseous byproduct of the plasma is highly reactive and hence severely restricts the use of mercaptosilane for PECVD in the large scale industrial production. A calorimetric based quantification of plasma deposited coatings revealed that the functional groups were present both in the bulk and on the surface.[48] However, the availability of the functional groups for biomolecule immobilization will depend on the density of packing, porosity (if any) and swelling. The peaks corresponding to carboxyl groups in PMIRRAS arises from both the surface and bulk composition, while the XPS data is only related to surface composition. For TA coating (Figure 2 top), PMIRRAS indicates the presence of C═O, from acrylic acid, in the bulk and/or surface. In XPS spectra (Figure 3 top), presence of O−C═O is also detected. So the carboxy groups are present at both surface and bulk. For MA coating (Figure 2 top), PMIRRAS indicates the presence of C═O in the bulk and/or surface. However, in the XPS data (Figure 3 middle), the O−C═O content is very low at the surface. So the main contribution for COOH peak in PMIRRAS is from the bulk in MA coating.

Figure.4 shows the secondary ion mass spectroscopic (SIMS) depth profile measurement of both TA and MA films. Mass/charge ratio (m/z) of 12 and 27.97 correspond to carbon and silicon, respectively in TA (Figure 4a, c) and MA (Figure 4b, d). It is observed in the SIMS depth profile measurements that both TA and MA coatings top layers are carbon rich (Figures 4a, b). Deeper in the film, the carbon content decreases. Oppositely, the surface silicon content of both coatings is very low and progressively increases (Figure 4c, d). As both TA and MA films are sequential depositions, the interface between MPTMS and AA layers is silicon-rich.

This illustrates what is believed to be a key characteristic of the surface coatings prepared by this method: they are graded in composition, being silica-rich near the substrate interface, carbon-rich and highly functionlized near the outer surface. Grading of the layer composition is achieved as a consequence of ion-induced mixing of the surface coating, under the application of the plasma. A higher Si content and lower C content at the interface could possibly be explained by oxidation of TEOS from its own oxygen and the residual oxygen from the pretreatment. Oxidation of the TEOS precursor results in formation of SiO_2 that deposits at the surface and CO_2 and H_2O in the bulk plasma that are pumped out of the chamber. A similar process can be assumed for MPTMS molecules.

The SIMS depth profile measurement of the silicon content of TA shows an increasing trend and decreases significantly as we go deep inside the film. Whereas for the MA coating, the silicon content is very low at the surface, then increases throughout the layer This is intrinsic to the deposition method used: a successive deposition of an intermediate layer (MPTMS or TEOS) and a reactive layer (AA). This is the reason why carbon content decreases while penetrating inside the layers (both TA and MA) in panels a and b in Figure 4. The same observation can be obsevred for MA coating while analyzing the silicon content. However, the silicon content of TA coating as measured by SIMS is very low at the top surface, then increases sharply to reach a maximum after, then slightly decreases. This decrease in the Si content can be due to a thickness effect. Indeed, Both layers do not have the same thickness (as a variation in coating growth rate): 8 nm for TA and 16 nm for MA coatings. As we approach the coating/gold interface, we can expect a slight decrease in Si content, which is observed in TA coating. This is not observed in MA coating because the coating is thicker and we do not reach the coating/gold interface.

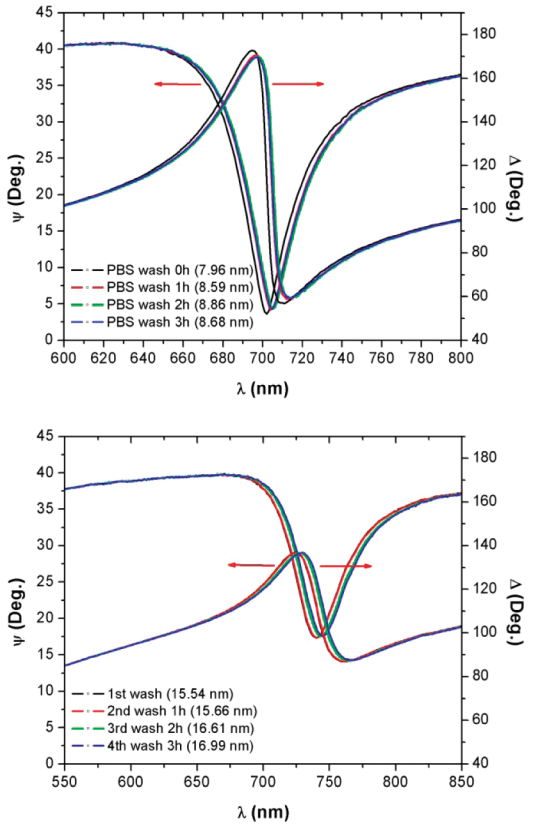

Figure 5. Stability studies of (top) TA and (bottom) MA coatings on gold surface tested under surface plasmon enhanced ellipsometry (SPEE) by exposing the surface to PBS for 3 h.

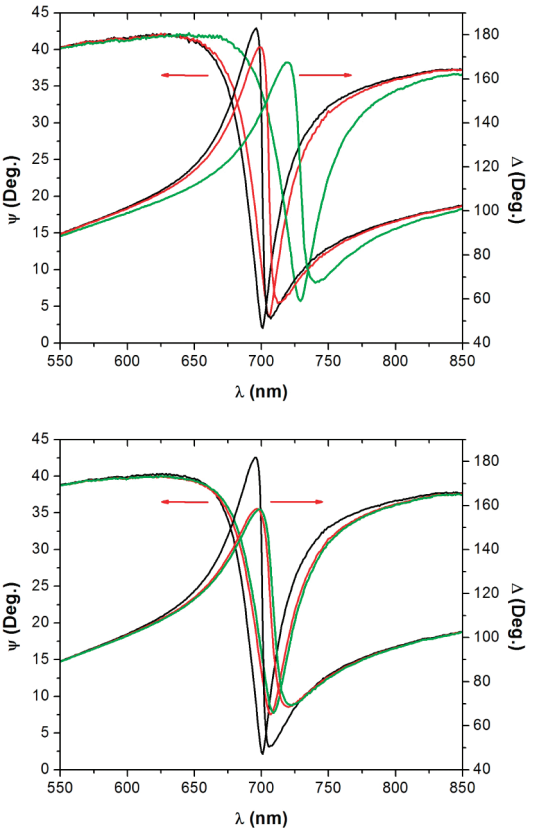

Figure 6. (Top) Ψ and Δ spectral shifts after binding of the capture of miR-16 probe and hybridized with complementary miR-16 target ssDNA. (Bottom) Ψ and Δ spectral shifts were only observed for binding of the capture miR-16 probe but not for the mismatched miR-195 target. (Black) Ψ and Δ spectral measurement after 1st PBS wash, (red) Ψ and Δ spectral measurement after the miR-16 probe binding (green, left) Ψ and Δ spectral measurement after the miR-16 target (green, right) Ψ and Δ spectral measurement after the mismatch miR-195 target.

2. Film Stability. The stability of both TA and MA films on Au-coated glass substrates under phosphate buffer saline (PBS, pH 7.4) washing inside a flow-cell were tested using surface plasmon enhanced ellipsometry (SPEE) (Figure 5).[27] In both cases, the SPR wavelengths were observed between 700 and 750 nm. The MA coating SPR wavelength is however higher than that of the TA coating. Obviously, the MA coating is thicker than TA one for which the SPR wavelength is shifted nearer to the infrared region.[49] The films were then washed with PBS every hour for up to 3 h and the film thickness changes were measured by ellipsometric fitting before and after every wash.

As a SPR signal is still observed after washing and does not highlight any film thickness decrease on washing, it can be deduced that both films have good adhesion and stability on exposure to aqueous solutions, which is essential for SPR-based techniques. However, the film thickness increased to about 0.72 nm and 1.45 nm for TA and MA coatings, indicating that the films swells under liquid environments (Figure 5). The film swelling upon exposure to the aqueous solution could result in a local porous structure forming at the surface.

3. Surface Reactivity and Biosensor Application. The reactivity of the coating was first checked through DNA attachment. Then performances of the created platform as a biosensor is demonstrated through DNA hybridization. Finally applicability to SPR-based detection is perfomed through bioassays using Biacore 3000 SPR instrument. The following experiments were only performed on TA coatings as above-mentionned characterization results highlighted a poor surface −COOH content of the MA films. The DNA hybridization was carried out using a miR-16 probe and a miR-16 target on TA coating deposited on gold on glass.

The thickness increase upon binding of the probe was 1.27 nm corresponding to a spectral shift in Figure 6, left (Spectral shift black to red). After miR-16 target incubation, the DNA hybridization resulted in a drastic thickness increase to reach 7.34 nm (Figure 6, left, spectral shift red to green).A small thickness increase after probe immobilization suggests that the ssDNA probes form a layer composed of coiled oligonucleotides, which are being stretched out during the hybridization to its complementary strand, resulting in a substantial thickness increase. This is in good agreement with previously reported results.[50,51] Figure 6, right, shows the spectral shift (spectrum black to red) upon binding of miR-16 probe. Upon addition of mismatch miR-195 target, there was no spectral shift as seen in Figure 6, right (overlapping of red and green spectra) demonstrating the fact that no hybridization took place and that there was no non-specific binding.

The applicability of the developed platform to other substrate, as well as their use in SPR based detection system is demonstrated below. The bioasssay performance obtained on plasma polymerized TA coatings deposited gold on polycarbonate was demonstrated using a Biacore 3000 SPR instrument and its

Table 3. Immunoassay on TA/Au/PC and Commercial CM5 Dextran Chip Performed on Biacore 3000 SPR System

	RL[a] (anti-IgG)	MD[b] (ng/mm^2)	RU albumin)	MD (ng/mm^2)	RU (IgG)	MD (ng/mm^2)	blank response	NSB of fibrinogen (1 mg/mL) (in ng/mm^2)
PECVD coatings	3874.0	3.9	1200	1.2	588 (15 ng/mL)	0.6	15 RU (0.015 ng/mm^2)	0.14
					905 (35 ng/mL)	0.9		
					1222 (70 ng/mL)	1.2		
CM5 dextran chips	7149.0	7.2	20	0.02	810 (15 ng/mL)	0.8	10 RU (0.010 ng/mm^2)	0.06
					1369 (35 ng/mL)	1.4		
					2108 (70 ng/mL)	2.1		

[a] Mass density was calculated using the conversion factor of 1000 RU = 1 ng/mm^2. (this corresponds to a 1° change in SPR angle). [b] The blank control was performed by injecting goat IgG over the antimouse IgG-immobilized surface.

performance was compared to the commercially available CM5 Biacore chips (Table 3). The standard EDC/NHS attachment protocol was used for antibody binding to coating surface. The high response unit signal measured after antibody attachment compared to blank signal first confirms once again the reactivity of the elaborated surface. Then, after incubation with the appropriate antigen, a linear relationship between response unit measured and antigen concentration can be observed. This confirms that the plasma polymerized carboxylic functionalities on gold on plastic can also be used in place of the conventional liquid-phase coated glass slides for SPR bioassays. Moreover, as the analytical performance of an assay procedure is often determined by nonspecific binding, the binding of nonanalyte constituents of the sample is critical. Hence we have measured the binding of fibrinogen, a protein constituent of serum that strongly adsorbs on surfaces. A significantly small amount of fibrinogen binding (0.14 ng/mm^2), even at very high fibrinogen concentration (1 mg/mL) confirms that protein nonspecific binding on the plasma polymerized carboxylic chips are very low.

A direct comparison of the performances of plasma-polymerized coatings to that of commercially available, liquid phase chemistry deposited, carboxy detran coatings of CM5 Biacore chips is performed. Both the reactivity to biomolecular ligand for covalent coupling and the nonspecific binding properties of the plasma polymerized chips are in comparison in terms of its performance to commercially available Biacore CM5 chips. The major difference between both chips is that the density of loading of primary antibody is very high in the case of BIACORE chips compared to that of the plasma deposited coatings. This apparently results in higher amount of antigen binding as is evidenced in Table 3. The reason for the observed low density of primary antibody loading in plasma deposited coatings is speculated to be the film thickness. The thickness of BIACORE chips is 100 nm and that of ours is 8 nm. The CM5 is a three-dimensional dextran matrix where antibody can bind all along the porous dextran coating whereas in 8 nm thick coating the antibody binding is restricted to top surface. The analytical performance of an assay procedure is often determined by nonspecific binding. For label-free methods such as SPR, the binding of nonanalyte constituents of the sample is critical. Hence we have measured the binding of fibrinogen, a protein constituent of serum that is strongly adsorbed on surfaces. Table 3 (Right) compares the plasma-coated chip to the CM5 chip in respect of the signal induced by a large excess of fibrinogen: the performance of the two preparations was again comparable. In both cases, the signal was significantly lower than the specific analyte signal, though non-negligible.

The room-temperature deposited plasma-based biosensor platform is advantageous in terms of its applicability on both gold-coated glass and nonglass surfaces and the quantity of surface carboxy groups are superior in non-thiol-based plasma-polymerized chips.

CONCLUSION

The low-temperature and solventless plasma polymerization process, with sequential deposition of siloxane and acrylic acid, is effectively used for functionalizing gold surfaces with a high retention of carboxylic functionality. Both the thiol-based (MPTMS) and non-thiol-based (TEOS) precursors were used as base layer for further functionalization with AA. The comparison of these films composition reveal a higher carboxylic content in TA films, probably due to a higher oxygen content in TEOs molecules as well as the presence of residual oxygen in the chamber. Moreover, the depth profile SIMS measurements highlighted that the films are graded in composition, being silica-rich near the substrate interface, being carbon-rich and highly functionlized near the outer surface. Using ellipsometric measurements, the coating stability and reactivity were demonstrated. Further, the biosensor applicability of the created platform through DNA hybridization experiments was performed based on SPEE detection system. Finally, the extension of the deposition process to polymeric substrates was successfully revealed on a SPR Biacore 3000 instrument. Comparison with commercial best-practice chips (Biacore CM5 dextran-coated gold on glass) demonstrated similar performance in respect of both specific (an IgG assay) and nonspecific (fibrinogen) adsorption. SPR based detection being one of the fastest growing techniques that is being explored for point of care based detections, the applicability of plasma polymerization with less than 5 min of functionalizing time and room-temperature storage of functionalized chips, for industrial bulk processing of SPR chips will be of very high importance. This study has shown that the high-speed, room-temperature, stable, reliable, and solventless plasma polymerization process with sequential deposition of organosilane (as adhesion layer) and acrylic acid (as anchoring layer) can lead to the emergence of new SPR-based biosensor platforms that can potentially replace the wet-chemistry-prepared coatings currently used.

ASSOCIATED CONTENT

Supporting Information. The XPS survey spectrum, high-resolution C 1s and Si 2p core level spectra of TA and MA coatings, as well as SPR kinetic data from Biacore 3000 SPR instrument are given in the Supporting Informations. "This material is available free of charge via the Internet at http://pubs.acs.org."

AUTHOR INFORMATION

Corresponding Author

*E-mail: ramprasad.gandhiraman@dcu.ie. Phone: +353 1 7007984. Fax: +353 1 7006558.

Present Address

▽CSIRO Materials Science and Engineering, Private Bag 33, Clayton South MDC, VIC 3169, Australia.

ACKNOWLEDGMENT

This material is based upon works supported by the Science Foundation Ireland under Grant 10/CE/B1821 DEW is an ETS Walton visiting fellow of Science Foundation Ireland. The authors thank Rajani K.V. for helping in the magnetron sputtering system for gold deposition and Prof. Z. Mekhalif for access to PMIRRAS facilities. C.V. is a postdoctoral researcher of the Belgian Fund for Scientific Research F.R.S.-FNRS.

REFERENCES

(1) Liedberg, B.; Nylander, C.; Lunstrom, I. *Sens. Actuators* **1983**, *4*, 299–304.

(2) Homola, J. *Chem. Rev.* **2008**, *108*, 462–493.

(3) Pirrung, M. C. *Angew. Chem., Int. Ed.* **2002**, *41*, 1276–1289.

(4) Jonkheijm, P.; Weinrich, D.; Schröder, H.; Niemeyer, C. M.; Waldmann, H. *Angew. Chem., Int. Ed.* **2008**, *47*, 9618–9647.

(5) Hodneland, C. D.; Lee, Y.-S.; Min, D.-H.; Mrksich, M. *Proc. Natl. Acad. Sci. U.S.A.* **2002**, *99*, 5048–5052.

(6) Garcıa-Aljaro, C.; Munoz, F. X.; Baldrich, E. *Analyst* **2009**, *134*, 2338–2343.

(7) Brockman, J. M.; Frutos, A. G.; Corn, R. M. *J. Am. Chem. Soc.* **1999**, *121*, 8044–8051.

(8) Love, C. J.; Estroff, L. A.; Kriebel, J. K.; Nuzzo, R. G.; Whitesides, G. M. *Chem. Rev.* **2005**, *105*, 1103–1170.

(9) Boujday, S.; Bantegnie, A.; Briand, E.; Marnet, P.-G.; Salmain, M.; Pradier, C.-M. *J. Phys. Chem. B* **2008**, *112*, 6708–6715.

(10) Mendoza, S. M.; Arfaoui, I. M.; Zanarini, S.; Paolucci, F.; Rudolf, P. *Langmuir* **2007**, *23*, 582–588.

(11) Vericat, C.; Vela, M. E.; Benitez, G.; Carro, P.; Salvarezza, R. C. *Chem. Soc. Rev.* **2010**, *39*, 1805–1834.

(12) Gandhiraman, R. P.; Volcke, C.; Gubala, V.; Doyle, C.; Basabe-Desmonts, L.; Dotzler, C.; Toney, M. F.; Iacono, M.; Nooney, R. I.; Daniels, S.; James, B.; Williams, D. E. *J. Mater. Chem.* **2010**, *20*, 4116.

(13) Volcke, C.; Gandhiraman, R. P.; Gubala, V.; Cummins, Th.; Fonder, G.; Nooney, R. I.; Mekhalif, Z.; Daniels, S.; Cafolla, A. A.; Williams, D. E. *Biosens. Bioelectron.* **2010**, *25*, 1875–1880.

(14) Slocik, J. M.; Beckel, E. R.; Jiang, H.; Enlow, J. O.; Zabinski, J. S., Jr.; Bunning, T. J.; Naik, R. R. *Adv. Mater.* **2006**, *18*, 2095–2100.

(15) Szunerits, S.; Rich, S. A.; Coffinier, Y.; Languille, M.-A.; Supiot, P.; Boukherroub, R. *Electrochim. Acta* **2008**, *53*, 3910–3915.

(16) Szunerits, S.; Boukherroub, R. *Langmuir* **2006**, *22*, 10716–10722.

(17) Szunerits, S.; Castel, X.; Boukherroub, R. *J. Phys. Chem. C* **2008**, *112*, 15813–15817.

(18) Touahir, L.; Niedzi, J.; Jonsson, K.; Galopin, E.; Boukherroub, R.; Gouget-Laemmel, A. C.; Solomon, I.; Petukhov, M.; Chazalviel, J.-N.; Ozanam, F.; Szunerits, S. *Langmuir* **2010**, *26*, 6058–6065.

(19) Wijaya, W.; Lenaerts, C.; Maricot, S.; Hastanin; Habraken, S.; Vilcot, J.-P.; Boukherroub, R.; Szunerits, S. *Curr. Opin. Solid State Mater.* **2011**, *15*, 208–224.

(20) Singh, B. K.; Hillier, A. C. *Anal. Chem.* **2008**, *80* (10), 3803–3810.

(21) Malic, L.; Cui, B.; Tabrizian, M.; Veres, T. *Opt. Express* **2009**, *17* (22), 20386–20392.

(22) Liu, C.; Cui, D.; Li, H. *Biosens. Bioelectron.* **2010**, *26*, 255–261.

(23) Coyle, C.; Gandiraman, R. P.; Gubala, V.; Le, N. C. H.; O'Mahony, C. C.; Doyle, C.; James, B.; Swift, P.; Daniels, S.; Williams, D. E. *Plasma Process. Polym.* **2011**, In press. DOI: 10.1002/ppap.201100070

(24) Gandhiraman, R. P.; Karkari, S. K.; Daniels, S.; MacCraith, B. D. *Surf. Coat. Technol.* **2009**, *203*, 3521–3526.

(25) Gubala, V.; Le, N. C. H.; Gandhiraman, R. P.; Coyle, C.; Daniels, S.; Williams, D. E. *Colloids Surf., B* **2010**, *81*, 544–548.

(26) Haïdopoulos, M.; Mirabella, F.; Horgnies, M.; Volcke, C.; Thiry, P. A.; Rouxhet, P.; Pireaux, J. J. *J. Microsc.* **2007**, *228*, 227–239.

(27) Le, N.C. H.; Gubala, V.; Gandhiraman, R. P.; Coyle, C.; Daniels, S.; Williams, D. E. *Anal. Bioanal. Chem.* **2010**, *398*, 1927–1936.

(28) Le, N. C. H.; Gubala, V.; Gandhiraman, R. P.; Coyle, C.; Daniels, S.; Williams, D. E. *Anal. Bioanal. Chem.* **2010**, *398*, 1927–1936.

(29) Nabok, A.; Tsargorodskaya, A.; Hassan, A. K.; Starodub, N. F. *Appl. Surf. Sci.* **2005**, *246*, 381–386.

(30) Poksinski, M.; Arwin, H. *Thin Solid Films* **2004**, *455−456C*, 716–721.

(31) Nabok, A.; Tsargorodskaya, A.; Holloway, A.; Starodub, N. F.; Demchenko, A. *Langmuir* **2007**, *23*, 8485–8490.

(32) Xu, H.; Lu, J. R.; Williams, D. E. *J Phys Chem B* **2006**, *110*, 1907–1914.

(33) Dreesen, L.; Silien, C.; Volcke, C.; Sartenaer, Y.; Thiry, P. A.; Peremans, A.; Grugier, J.; Marchand-Brynaert, J.; Brans, A.; Grubisic, S.; Joris, B. *ChemPhysChem* **2007**, *8*, 1071–1076.

(34) Finke, B.; Schröder, K.; Ohl, A. *Plasma Process. Polym.* **2009**, *6*, S70–74.

(35) Wavhal, D. S.; Zhang, J.; Steen, M. L.; Fisher, E. R. *Plasma Process. Polym.* **2006**, *3*, 276–287.

(36) Socrates, G. *Infrared and Raman Characteristic Group Frequencies*; Wiley VCH: Chichester, U.K., 2004.

(37) Retsch, M.; Walther, A.; Loos, K.; Müller, A. H. E. *Langmuir* **2008**, *24* (17), 9421–9429.

(38) Finocchio, E.; Macis, E.; Raiteri, R.; Busca, G. *Langmuir* **2007**, *23* (5), 2505–2509.

(39) Li, Y.-S.; Wang, Y.; Tran, T.; Perkins, A. *Spectrochim. Acta, A* **2005**, *61*, 3032–3037.

(40) Choudhury, T.; Jones, F. R. *Int. J. Adhes. Adhes.* **2006**, *26*, 79–87.

(41) Beamson, G.; Briggs, D. *High-Resolution XPS of Organic Polymers: The Scienta ESCA300 Database*, 1st ed.; John Wiley & Sons: Chichester, U.K., 1992.

(42) Detomaso, L.; Gristina, R.; Senesi, G. S.; d'Agostino, R.; Favia, P. *Surf. Coat. Technol.* **2005**, *200*, 1022–1025.

(43) Morel, A. L.; Volmant, R. M.; Methivier, C.; Krafft, J. M.; Boujday, S.; Pradier, C. M. *Colloids Surf., B* **2010**, *81*, 304–312.

(44) Fatyeyeva, K.; Bigarré, J.; Blondel, B.; Galiano, H.; Gaud, D.; Lecardeur, M.; Poncin-Epaillard, F. *J. Membr. Sci.* **2011**, *366*, 33–42.

(45) Laibinis, P. E.; Whitesides, G. M.; Allara, D. L.; Tao, Y. T.; Parikh, A. N.; Nuzzo, R. G. *J. Am. Chem. Soc.* **1991**, *113*, 7152–7167.

(46) Senkevich, J. J.; Mitchell, C. J.; Yang, G.-R.; Lu, T.-M. *Langmuir* **2002**, *18*, 1587–1594.

(47) Singh, J.; Whitten, J. E. *J. Phys. Chem. C* **2008**, *112*, 19088–19096.

(48) Gubala, V.; Gandhiraman, R. P.; Volcke, C.; Doyle, C.; James, B.; Daniels, S.; Williams, D. E. *Analyst* **2010**, *135*, 1375–1381.

(49) Arwin, H.; Poksinski, M.; Johansen, K. *Appl. Opt.* **2004**, *43*, 3028–3030.

(50) Liebermann, T.; Knoll, W.; Sluka, P.; Herrmann, R. *Colloids Surf., A* **2000**, *169*, 337–350.

(51) Larsson, C.; Rodahl, M.; Hook, F. *Anal. Chem.* **2003**, *75*, 5080–5087.